

Beam-beam phenomena in the Tevatron

T. Sen
FNAL

1 Introduction

Protons and anti-protons in the Tevatron circulate on separated helical orbits within the same beam pipe and collide at two experimental detectors CDF and D0. Electrostatic separators placed at several locations create these helical orbits. In Run I there were six bunches per beam. In Run II, which started in April 2001, each beam has three trains of twelve bunches. Consequently there are six times as many long-range beam-beam interactions as in Run I. It was anticipated and observed that these long-range beam-beam interactions would have a more serious impact on beam lifetime and losses. Table 1 contains a brief list of the important parameters.

After a slow start partly due to the impact of the long-range interactions, the luminosity in Run II has been steadily increasing over time. Figure 1 shows the luminosity evolution over the past few years. In 2004, the Tevatron surpassed the luminosity goals set for the 1st stage of Run II. The record until now was set on July 16, 2004 when the average initial luminosity exceeded $10^{32}\text{cm}^{-2}\text{sec}^{-1}$. Several improvements in the injectors and the Tevatron made this possible, see Reference [1] for more details.

A collider fill starts with coalesced proton bunches from the Main Injector loaded one bunch at a time onto the central orbit in the Tevatron. The electrostatic separators are powered after all 36 proton bunches are loaded and the protons are moved to their helical orbit. Anti-protons are loaded four bunches at a time into one of three abort gaps onto the anti-proton helical orbit. The anti-proton bunches are moved longitudinally relative to the proton bunches (“cogged”) to make room for the next four bunches in the abort gap. After each train is full the two beams are accelerated to top energy. A final cogging is done at the end of the acceleration. The optics is changed to lower the beta functions at the IPs from 1.6m to 0.35m. After the final step of this beta squeeze, the transverse separations at the IPs are reduced to zero with the use of the appropriate separators around the IPs. Collimators are moved in to reduce the beam halo and background in the detectors and a store begins.

The configuration of beam-beam interactions is different at injection and collision. Each bunch experiences 72 long-range interactions at injection but at collision there are 70 long-range interactions and two head-on collisions per bunch. In total there are 138 locations around the ring where beam-beam interactions occur. The sequence of 72 interactions out of the 138 interactions is different for each bunch, hence the effects are different from bunch to bunch. The locations of these interactions and the beam separations change from injection to collision. The left plot in Figure 2 shows the separations at all 138 interaction points in the ring after the 2nd cogging at injection.

Parameter	Injection (p/\bar{p})	Collision (p/\bar{p})
Circumference [m]	6283.187	
Number of bunches	36	
Bunch spacing [nsec]	396	
Energy [GeV]	150	980
Beta* at IP [m]	1.6	0.35
Normalized transverse emittance (95 %)[$\pi\text{mm-mrad}$]	20/15	
Bunch intensity ($\times 10^{11}$)	2.5/0.36	
Bunch length [cm]	80	48
Beam-beam parameter	0.0018/0.0092	

Table 1: Selected beam parameters in the Tevatron

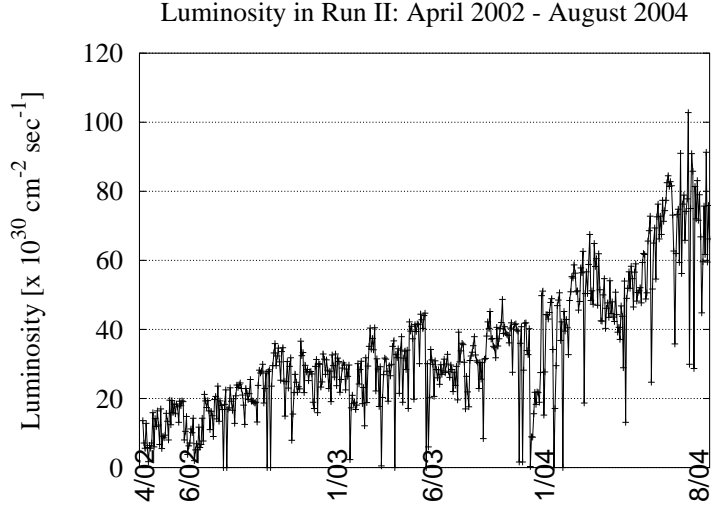


Figure 1: Evolution of the initial luminosity (averaged over CDF and D0) in Run II.

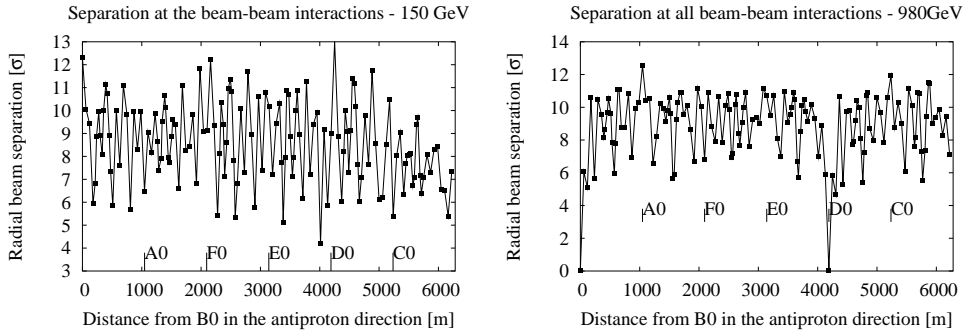


Figure 2: Left: Radial beam separations at 138 interaction points around the ring. Left: At injection (150 GeV) after the second cogging. Right: At low-beta (980 GeV). The head-on collisions are at locations B0 and D0.

The minimum separation is about 4σ . The right plot in this figure shows the beam separations at collision. The head-on collisions occur at B0 (CDF experiment) and D0 (D0 experiment). The minimum separations ($\sim 5\sigma$) at the parasitic encounters occur close to the experiments.

2 Theory and Observations

Head-on beam-beam interactions are often characterized by a single parameter - the head-on beam-beam tune shift. This is the tune shift of a small transverse amplitude particle and it is also a measure of the beam-beam induced tune spread in the bunch. These head-on interactions drive only even order resonances so the tunes in colliders are chosen such that the tune footprint does not straddle low even order resonances. While much is understood about head-on interactions, several phenomena lack quantitative predictions, e.g. emittance growth with mismatched beams. Long-range interactions are more complex than the head-on interactions. In addition to changing the tunes, these interactions in general also change the orbits, coupling and chromaticity. As with the tune changes, the orbit, coupling and chromaticity changes are amplitude dependent. The long-range interactions drive both even and odd order resonances. The changes in orbits, tunes, coupling, chromaticity, resonance strengths depend on several parameters including: beam separations, plane of the helix, beam emittance, beta functions, dispersion, phase advances between the interactions etc. If for example, the phase advances between the parasitics can be adjusted with independently powered quadrupoles as is done in CESR, then the resonance strengths can be significantly

altered. Quadrupoles in the Tevatron are on the same bus as the main dipoles, thus ruling out that option. Instead the most direct way of minimizing the impact of the long-range interactions in the Tevatron is by manipulating the helix configuration, lower beam emittances, reduction of chromaticities and careful control of the tunes of both beams.

A first step is understanding how quantities like tune shifts, coupling, chromaticity, resonance strengths depend on beam parameters. Detailed discussions may be found in Reference [2]. For illustrative purposes it is useful to consider round beams for which the expressions simplify. The tune shifts, the strength of the coupling resonance and chromaticity shifts at small amplitudes due to a single long-range beam-beam interaction where the separations are large (compared to the beam size), the beams are round and $\beta_x = \beta_y$ are given by

$$\Delta\nu_x(0,0) = \frac{N_p r_p}{2\pi\epsilon_p^N} \frac{\cos 2\theta}{d^2} \quad (1)$$

$$F_{1,-1,p}(0,0) = -\frac{N_p r_p}{\pi\epsilon_p^N} \frac{\sin 2\theta}{d^2} \exp[i(\psi_x - \psi_y - (\nu_x - \nu_y - p)\frac{s}{R})] \quad (2)$$

$$\nu'_x(0,0) = 2\frac{N_p r_p}{\pi\epsilon_p^N} \frac{1}{d^3} [\tilde{\eta}_x \cos 3\theta + \tilde{\eta}_y \sin 3\theta] \quad (3)$$

Here N_p is the proton bunch intensity, r_p is the classical proton radius, ϵ_p^N is the normalized proton emittance, θ is the angle of the plane of the helix, d is the beam separation in units of the rms proton beam size, ψ_x, ψ_y are the phase advances, ν_x, ν_y are the tunes and $\tilde{\eta}_x, \tilde{\eta}_y$ are the dispersions in units of the rms beam sizes. At large distances, both the tune shift and the coupling fall as $1/d^2$ while the chromaticity falls off more rapidly as $1/d^3$. The energy dependence is contained mainly in the scaled distance d . If there were enough separator strength to keep the physical separation between the two beams constant at different energies, then $d \propto \sqrt{E}$ and the above parameters would decrease with energy. If instead the scaled separation d is kept constant, as is done during the acceleration from 150 GeV to ~ 500 GeV, the above parameters are independent of energy. At energies above 500 GeV, the separator voltages stay at constant values close to their maximum. Consequently d decreases as $1/\sqrt{E}$ and the parameters increase with energy. These optical parameters have different dependencies on the helix angle θ . For example at 45° , the tune shift vanishes but the coupling is a maximum. If the vertical dispersion is zero, the chromaticity vanishes only if $\theta = 30^\circ, 90^\circ$.

From analytical calculations we find that at 150 GeV, the tune shifts and coupling due to the beam-beam interactions are much smaller than due to the machine nonlinearities. Chromaticity and resonance strengths are however significant. At low-beta and 980 GeV, the tune shift (and spread) and resonance strengths are dominated by the contributions of the beam-beam interactions. Effects due to synchro-betatron resonances are important because of the large momentum spread in the beams and relatively large chromaticities. These resonances are individually of small width but are numerous and their overlap can transport particles to large amplitudes.

While these calculations yield insight, they do not provide much information on the evolution of the beams over time. Numerical simulations offer a way to follow particle motion in fields as complex as those in the Tevatron. Dynamic aperture calculations for protons and anti-protons have been done with various tracking codes, e.g. MAD, SIXTRACK, TEVLAT. Lifetime calculations for anti-protons with only beam-beam fields done by colleagues at LBNL and SLAC have also been reported earlier [3]. A simulation code BBSIM [4] has been recently developed at FNAL for calculating lifetimes, diffusion coefficients, beam profiles and emittance growth. Another code LIFETRACK developed several years ago at Novosibirsk, Russia is also being adapted for similar purposes. These lifetime codes make use of the parallel processing features now available with either PC clusters or at the NERSC supercomputing facility.

Dynamic apertures calculated by simulation were found to be in good agreement with measured dynamic apertures when the Tevatron was operated at large chromaticities of (8,8) units. Lifetime simulations at injection showed that the lifetime was sensitive to the chromaticity setting, in agreement with observations. Lifetime simulations at collision are now aimed at reproducing the observed variations in bunch to bunch lifetimes and emittance growth and finding ways to limit the effect of beam-beam interactions.

Tevatron performance over the past two years is summarized in Table 2. We discuss beam-beam observations at each stage of the operational cycle in more detail below. Discussions of beam-beam phenomena may also be found in References [5], [6] and in several reports available on the Fermilab Accelerator Division document database [7].

	10/02	08/03	08/04	pbar/p only
Maximum Luminosity $\times 10^{30}$	36	52	99	NA
Maximum Protons/bunch at low-beta [$\times 10^9$]	170	266	257	266
Maximum Pbars/bunch at low-beta [$\times 10^9$]	19	28	34	30
Pbar loss at 150 GeV	13%	2%	5%	2%
Proton loss at 150 GeV	14%	8%	5%	5%
Pbar loss during the ramp	8%	8%	7%	2%
Proton loss during the ramp	11%	5%	4%	3%
Pbar loss during the squeeze	2%	2%	4%	0%
Proton loss during the squeeze	2%	1%	2%	0%
Pbar lifetime at start of store [hrs]	54	30	24	900
Proton lifetime at start of store [hrs]	77	29	110	300
Pbar efficiency 150 GeV \rightarrow low-beta	83%	82%	84%	96%
Proton efficiency 150 GeV \rightarrow low-beta	72%	83%	89%	92%

Table 2: Tevatron performance in October 2002, August 2003 and August 2004. These numbers are the averages over the respective months. The peak bunch intensities achieved during the record luminosity store on July 16th, 2004 were about 275×10^9 protons/bunch and 40×10^9 anti-protons per bunch. The data with either protons or anti-protons only were obtained during dedicated machine studies.

2.1 Injection

Anti-proton losses at injection were found to be strongly influenced by beam-beam effects until recently. During most of 2002 and the first half of 2003, the anti-proton losses with protons present were much larger, ranging from 10-15%. Lifetimes ranged between 1-5 hours. The anti-proton lifetime was found to depend on the anti-proton emittance, lower emittance bunches had longer lifetimes. Experiments with only anti-protons showed that the beam loss at 150 GeV was very small, about 2%. During the summer of 2003 several changes were made which greatly reduced the anti-proton losses from around 9% to 2%. These changes included smaller longitudinal anti-proton emittances from better coalescing in the Main Injector, lowering of chromaticity following the removal of the C0 Lambertson and introduction of the transverse dampers, lower currents in some feed-down sextupole circuits which reduced strong local nonlinearities and removal of SEMs from the injection lines which reduced the emittance blow-up. Beam-beam effects at 150 GeV now have very little influence on anti-proton losses.

Proton losses at injection have not been significantly influenced by the anti-protons. Instead the proton lifetime has largely been determined by the machine chromaticity and momentum spread. After the introduction of the transverse dampers, removal of the C0 Lambertson magnet, a significant source of impedance, and the installation of a liner in the F0 Lambertson, protons could circulate stably in the Tevatron with lower chromaticities. Lowering the chromaticities from 8-10 units to 2-4 units has improved the proton lifetime at 150 GeV. The small dynamic aperture on the proton helix due to the magnet nonlinearities and restricted physical aperture at a few locations are now the main sources of beam loss. While the impact of beam-beam interactions on protons has been small, nevertheless the proton lifetime does drop while anti-protons are loaded and proton losses are observed during cogging when the beam separations change.

2.2 Acceleration

Anti-proton losses during acceleration are strongly influenced by beam-beam interactions. On average anti-proton losses are about 6% higher when protons are present. The losses are observed to be well correlated with the vertical emittance, lower emittance bunches have lower losses. During the ramp the separator voltages increase linearly until about 500 GeV when the maximum voltage is reached. The beam separation, in units of the beam size, stays constant while the separator voltages are increasing but falls thereafter. As a consequence the significant portion of anti-proton losses are observed during the second half of the ramp. Helix solutions that increase the minimum separation in the last part of the ramp were commissioned in August 2003 and have lead to some improvement [8].

Proton losses during acceleration have remained around 5% over the past year. Beam studies have shown that the losses occur mostly in the early part of the ramp and depend strongly on the longitudinal emittance [9], the quality of coalescing in the Main Injector and more recently on the vertical emittance.

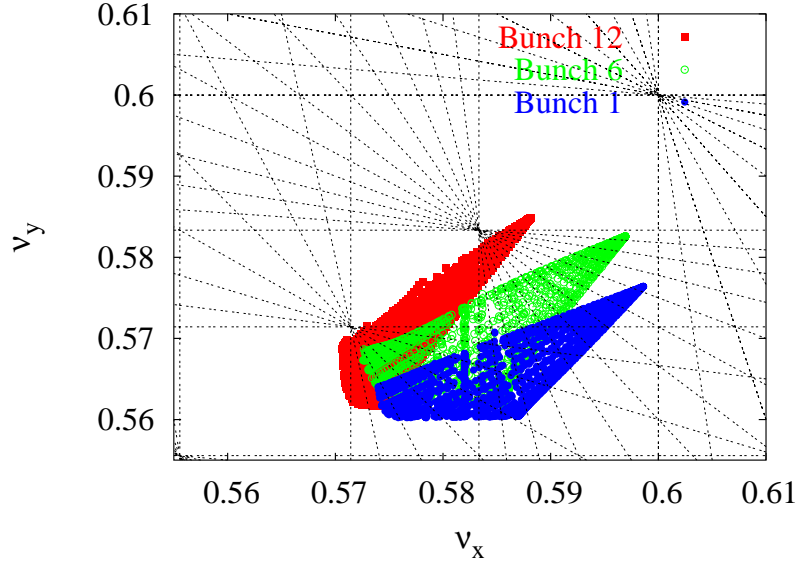


Figure 3: Tune footprint of anti-proton bunches 1, 6 and 12 in a train during collisions at 980 GeV. Sum resonances up to 12th order are also shown.

We expect that lowering the chromaticities during the acceleration will also help reduce losses. The use of octupoles and/or transverse dampers during the ramp will be commissioned in future beam studies. The beam separations will also be increased with additional separators.

2.3 Squeeze

Anti-proton losses were very large ($\sim 20\text{-}25\%$) until March 2002 during the step in the squeeze when the helix reverses polarity. At this stage, the minimum beam separation was less than 2σ . A helix solution was found that increased the beam separation at this point in the squeeze. That combined with a faster transition through this step reduced anti-proton losses significantly. Even with this helix the beam separation drops momentarily during the transition from the injection to the collision helix. There is some evidence of beam-beam related anti-proton losses ($\sim 2\%$) during the squeeze. Some of these losses occur during beam scraping done for 10 minutes after the beams are brought into collision following the squeeze. This scraping removes halo particles and results in about 1% beam loss in both beams.

Proton losses during the low-beta squeeze are usually not significant. Adjustments of the orbits and tunes have usually sufficed to control losses when they are occasionally large.

2.4 Collision

At collision, each bunch experiences 2 head-on collisions and 70 long-range interactions. The nominal working point ($\nu_x = 0.585, \nu_y = 0.575$) is chosen to lie between fifth and seventh order resonances. For anti-protons, the head-on collisions contribute a tune shift about 0.02 while all the long-range interactions contribute about 0.005. Fig. 3 shows the footprints due to the beam-beam interactions for bunch 1, 6, and 12 superposed on nearby sum resonances up to twelfth order. Footprints of bunches 2-11 are clustered around the footprint of bunch 6. The major differences in the tune shifts between bunch 6, and bunch 1 and 12 are due to the missed parasitic collision closest to the IP, upstream for bunch 1 and downstream for bunch 12. Due to the 3-fold symmetry, this pattern is repeated in the other two trains.

This bunch to bunch difference in tunes has now been experimentally measured in several stores with a new high frequency Schottky monitor [10]. Figure 4 shows the bunch by bunch tunes measured in a recent store and an analytical calculation of the tune shifts [2]. This pattern of tune shifts has been reproducibly observed in several stores. The analytical results predict both the scale of the tune shifts and the variation between bunches in

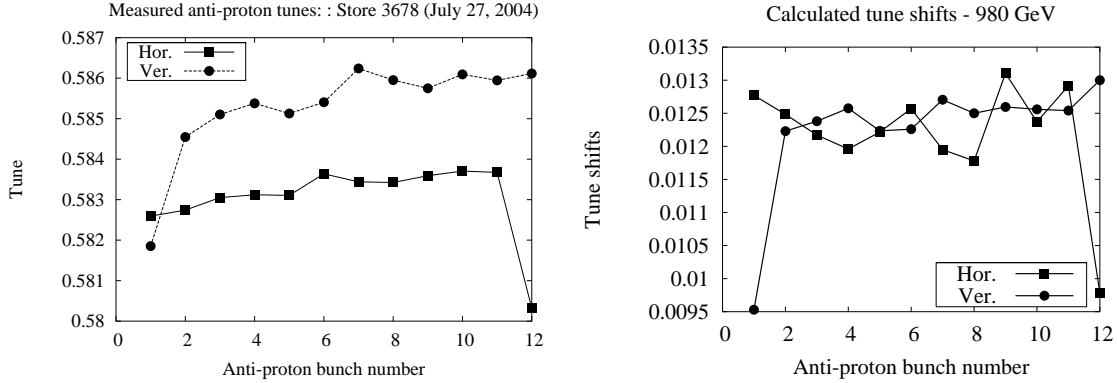


Figure 4: Left: Measured bunch by bunch tunes of anti-protons (courtesy of P. Lebrun), Right: analytical prediction of the centroid tune change within a bunch (right).

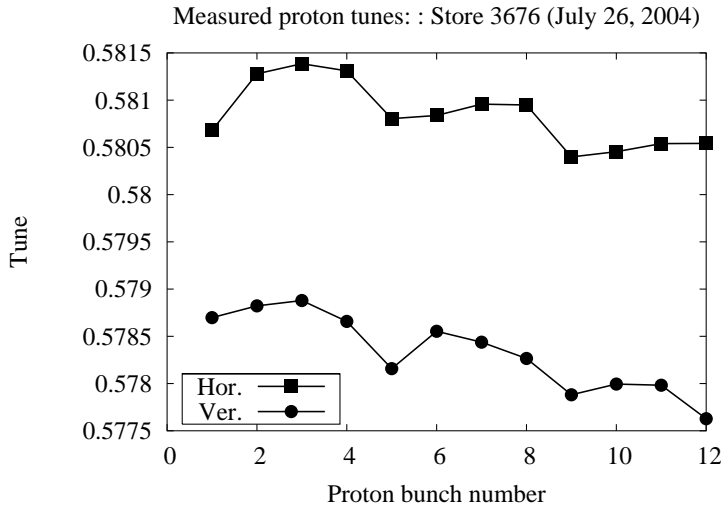


Figure 5: Measured bunch by bunch tunes of protons in a recent store (courtesy P. Lebrun).

both planes reasonably well. The residual differences are due to uncertainties in the optics, beam intensities and emittances. Bunch by bunch tunes of protons were measured recently in one store - see Figure 5. While the tune variations between bunches are small, these variations could be due to beam-beam effects from the anti-protons. The pattern of tune variation, roughly periodic over 4 bunches, follows the intensity distribution of the anti-protons - see Figure 7 for an example. The tune differences are however close to the resolution of the tune measurement - more such measurements are required to definitively attribute the shifts to beam-beam effects.

The long-range beam-beam interactions also have an impact on bunch to bunch orbits. A synchrotron light monitor is able to image individual proton and anti-proton bunches at collision [11]. Figure 6 shows the orbits of anti-protons as observed in an early store. The horizontal position of the anti-proton bunches shows the same trend in all three trains - as expected from the three-fold symmetry. The maximum spread in horizontal position is about 30 microns (in the first train) and closer to 20 microns in the other trains. The vertical spread is smaller than 20 microns in all trains. The spread in proton orbits is about a factor of 2-3 smaller. The observed orbit shifts agree well with analytical calculations of these shifts [12].

We now discuss the impact on beam lifetimes and emittances with the example of a store on August 18th, 2004 - one of the recent higher luminosity stores before the shutdown in August. Figure 7 shows the intensity distribution among the anti-proton and proton bunches in this store. Typically the average intensities of the first 4 anti-proton bunches in each train are larger than those of the following bunches in the train - these leading bunches are the first 12 anti-proton bunches to be injected. In this store the intensities of the last 4 bunches A33-A36 was

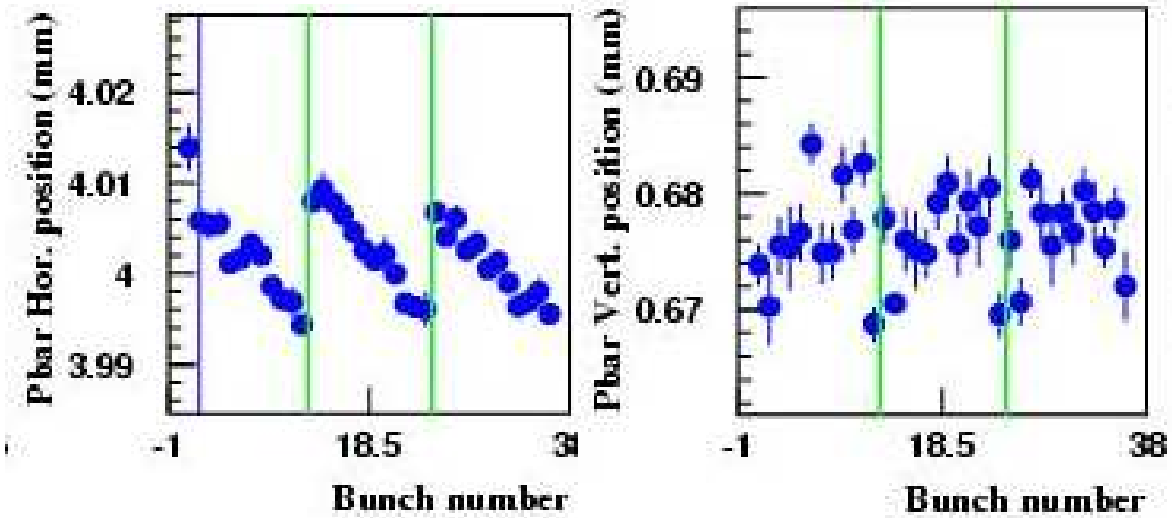


Figure 6: Positions of anti-proton bunches observed at the synchrotron light monitor in Store 1787. Long-range interactions are responsible for the differences in bunch to bunch orbits [12].

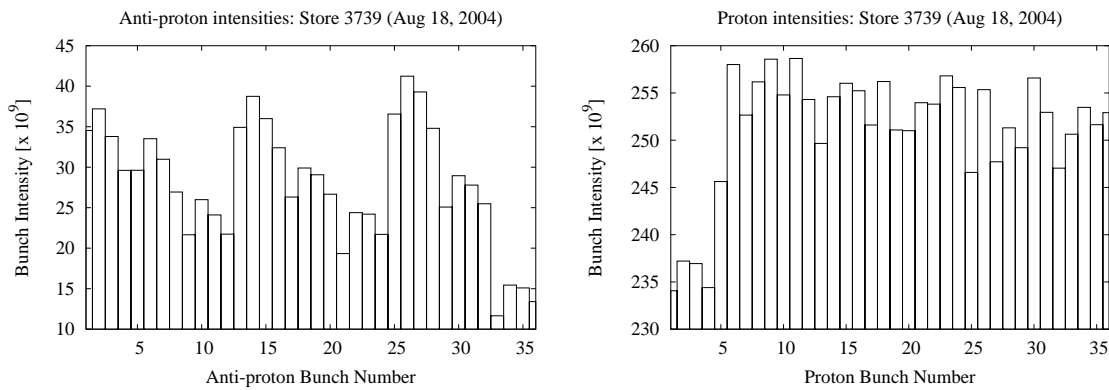


Figure 7: Bunch by bunch intensities at the start of Store 3739 (August 18, 2004). Left: anti-protons; Right: protons

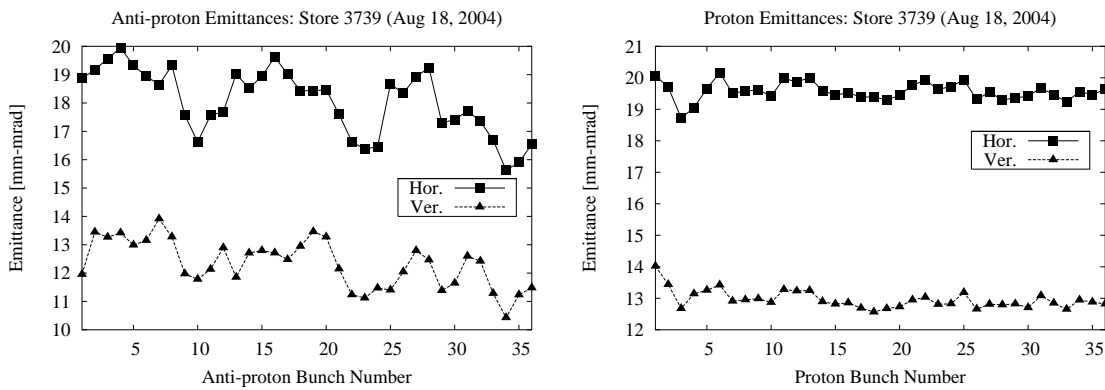


Figure 8: Bunch by bunch emittances at the start of Store 3739 (August 18, 2004). Left: anti-protons; Right: protons

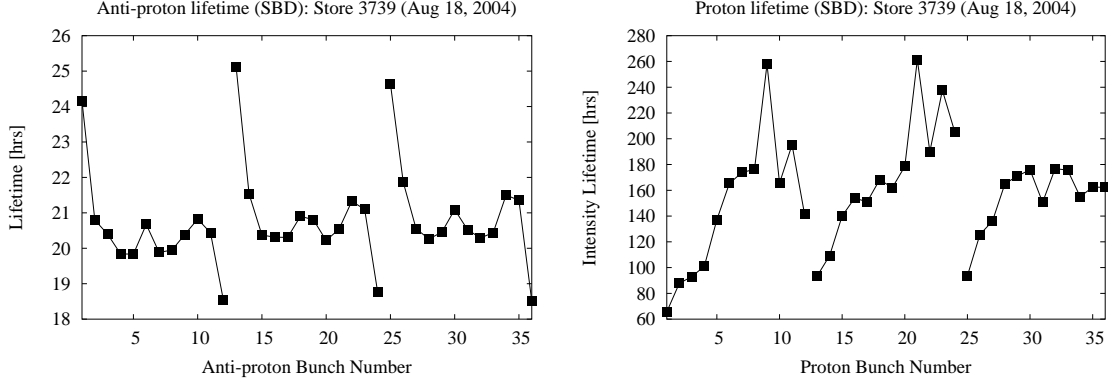


Figure 9: Intensity lifetimes, bunch by bunch, at the start of Store 3739 (August 18, 2004). Left: anti-protons; Right: protons. The gaps show the 3 trains of 12 bunches in each beam.

particularly low, thus the intensities over the whole beam varied by a factor of 4. The intensity distribution amongst proton bunches is typically more uniform, in this store the variation is about 10%. The emittance distribution is shown in Figure 8. The last 4 anti-proton bunches in each train typically have a lower emittance than the others, the range of variation in this store is about $4\pi\text{mm-mrad}$ for the normalized 95% emittance. The proton emittance distribution is much more uniform, the range of variation is about $1\pi\text{mm-mrad}$.

Figure 9 shows the bunch by bunch intensity lifetimes of both beams. This lifetime is mainly determined by the luminosity. Since the proton intensity and emittance distribution is relatively uniform, the 3-fold symmetry of the bunch structure is clearly reflected in the anti-proton lifetimes. This symmetry is somewhat broken in the lifetimes of the proton bunches. The lifetimes of the last 4 proton bunches in the first 2 trains, P9-P12 and P21-P24, are larger than those of P33-P36, the last 4 bunches in the 3rd train. This is a particular feature of this store since P9-P12 collided with the low intensity anti-proton bunches A33-A36 at D0, P21-P24 collided with these anti-proton bunches at B0 while P33-P36 do not collide with them anywhere but instead with the higher intensity bunches A21-A24 at B0 and bunches A9-A12 at D0.

The bunch lifetime related to dynamics (i.e. not related to luminosity) can be calculated as

$$\frac{1}{\tau_{Dy}(\bar{p})} = \frac{1}{\tau(\bar{p})} - \frac{1}{\tau_{\mathcal{L}}(\bar{p})} \quad (4)$$

$$\frac{1}{\tau_{\mathcal{L}}(\bar{p})} \equiv \frac{\mathcal{L}\sigma_{p\bar{p}}}{N_{\bar{p}}} = \frac{f_{rev}}{2\pi} \frac{N_p}{\beta^* \sqrt{(\epsilon_{x,p} + \epsilon_{x,\bar{p}})(\epsilon_{y,p} + \epsilon_{y,\bar{p}})}} \mathcal{H}\left(\frac{\beta^*}{\sigma_{s,eff}}\right) \sigma_{p\bar{p}} \quad (5)$$

Here ϵ are the transverse emittances, \mathcal{H} is the hourglass factor and $\sigma_{p\bar{p}}$ is the inelastic $p - \bar{p}$ scattering cross-section. Figure 10 shows the dynamic lifetime τ_{Dy} for both beams. Variations in these lifetimes are mainly due to beam-beam effects. The 3-fold symmetry is still present in the anti-proton dynamic lifetime - the only spoiler is bunch A25 which has a significantly lower dynamic lifetime than bunches A1 and A13 at the head of the other 2 trains. The dynamic lifetime of protons varies over a large range, between 120-800 hours, perhaps indicative of beam-beam effects on the protons as well. Longitudinal losses due to intra-beam scattering and rf noise may also account for some of the differences bunch to bunch. The lifetime due to scattering off the residual gas is in the range of 600-900 hrs at 980 GeV [13].

The transverse emittance growth times of proton bunches in this store were in the range from 14-21 hours with intra-beam scattering the dominant contributor. The anti-proton emittances grew at a much slower rate in this store. This has not always been the case. Until recently in some stores with relatively high proton intensities, large emittance growth was observed in most anti-proton bunches. The bunches at the head and tail of a train however had a lower emittance growth rate, so the emittance profile within a train had a scalloped shape - see Reference [1] for an example. This emittance growth was very sensitive to the tune setting - in recent stores, this problem seems to have been eliminated by small adjustments to the tunes.

Another clear manifestation of beam-beam effects on anti-protons is observed in the change of tunes during the store. The tunes change because of the intensity loss and emittance growth of the opposing beam. From the

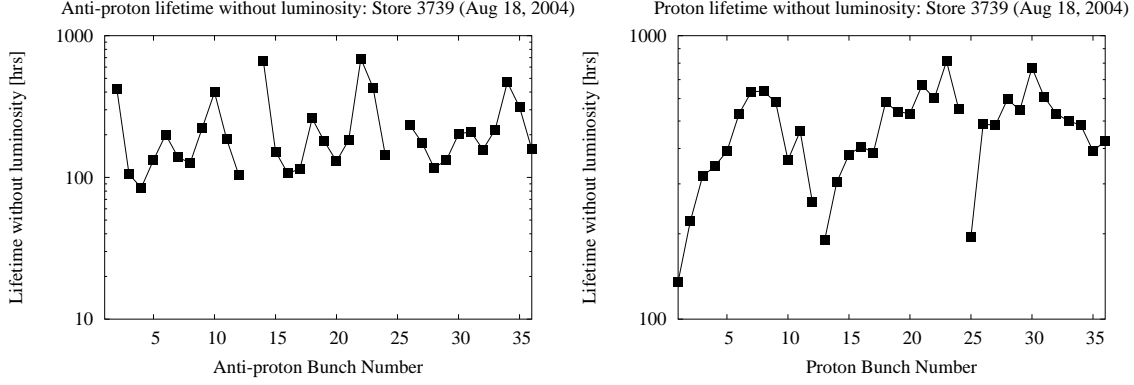


Figure 10: Lifetimes not related to luminosity losses for anti-protons (left) and protons (right). The lifetimes due to luminosity were subtracted from the intensity lifetimes as shown in Equation (4).

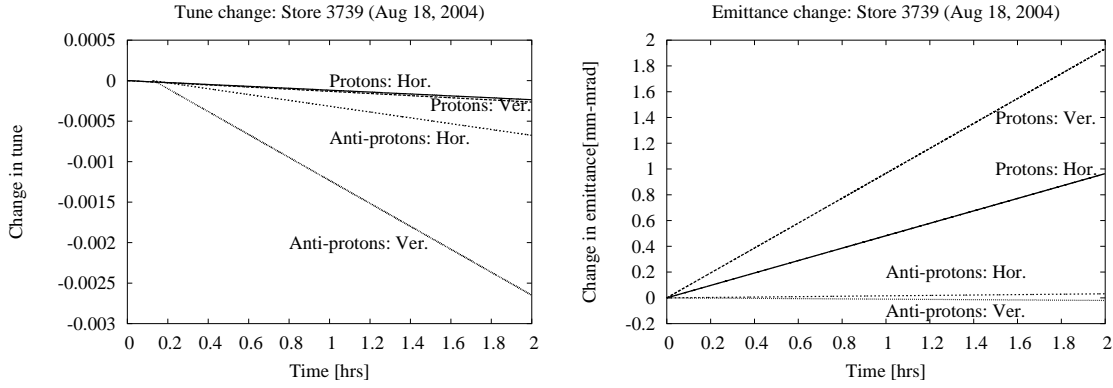


Figure 11: Changes in the average tunes(left) and emittance(right) during the first 2 hours of the store. The beam-beam related tune changes are related to the changes in the intensity and emittance of the opposing beam. For example, the larger anti-proton tune changes is well correlated with the larger growth of the proton emittances.

expression for the head-on tune shift, it follows that the rate of tune change of anti-protons, for example, is

$$\frac{d}{dt}\Delta\nu(\bar{p}) = -\xi(\bar{p})\left(\frac{1}{\tau_{\epsilon_p}} + \frac{1}{\tau_p}\right) \quad (6)$$

where $\xi(\bar{p})$ is the beam-beam parameter for anti-protons, τ_{ϵ_p} is the proton emittance growth time and τ_p is the proton intensity lifetime. The proton emittance growth has a larger impact on the anti-proton tune change because $\tau_{\epsilon_p} < \tau_p$. Conversely, the rapid intensity loss of anti-protons contributes more than the anti-proton emittance growth to the proton tune change. The left panel in Figure 11 shows the tune changes averaged over all bunches for both beams. The right panel in this figure shows the average emittance change over this same time. The fact that the anti-proton tune changes are larger correlates well with the larger emittance change of the protons.

A recent phenomenon with smaller anti-proton emittances and increasing anti-proton intensities has been the occasional large proton losses at the start of stores. These large losses were enough to significantly increase the background in the detectors. Analysis showed that typically proton bunches that collided with anti-proton bunches with the smallest vertical emittance had the largest losses. This suggests that losses are due to those protons which see the strongest part of the non-linear beam-beam force. These losses are also very tune dependent. Recently the proton tunes were placed between the 7th and 12th order resonances with the differential tune circuits. These changes have brought the initial proton losses under control.

3 Beam-beam compensation

Tevatron Electron Lens (TEL)

The TEL has been in operation since March 2001 and aims to compensate the tune spread between bunches at top energy. The electron gun was replaced in January 2003 by another gun which creates a smoother Gaussian profile of the electron beam. In studies with the electron lens acting on protons, the smoother field was found to preserve the lifetime of the protons and was a significant improvement over the previous gun which created a more rectangular profile. The alignment of the lens is very critical - for example the sign of the induced tune shift can change due to small changes in the orbit. In a beam study performed in a store where scallops had developed, the electron lens was successfully used to change the tunes of a selected anti-proton bunch and thereby reduce its emittance growth rate. The electron lens is also routinely used to remove coasting protons circulating in the ring by resonant excitation of particles in the abort gaps. It has also been used on occasion to tickle a bunch to increase the signal to noise ratio for a tune measurement. Further work on the electron lens to make it an operational device for tune shift compensation is continuing. The improvements required include better control of the electron lens orbit, improved stabilization of electron currents and perhaps a wider electron beam. More details can be found in Reference [1].

Wire Compensation

Compensation of the long-range interactions by steady current carrying wires was investigated for the Tevatron following a similar proposal for the LHC [14]. A preliminary investigation with four 1m long wires placed in four warm straight sections showed that the dynamic aperture of a selected anti-proton bunch at 150 GeV could be significantly increased by appropriate placement of the wires and carefully selected currents. More recent investigations at collision energy [15] showed that the wire compensation works only in ideal cases, e.g. when the beams are round and the wire can be placed at nearly the same betatron phase as the beam-beam interaction. The beams are not round at several of the long-range interactions in the Tevatron. In fact, the beams are highly elliptical (aspect ratio 4:1) at the parasitics closest to the IPs. These interactions cannot be well compensated with the field of round wires. Wires with elliptical cross-sections could be an alternative. However this project has been dropped from the Run II upgrade given its R& D nature and the limited time scale of Run II.

4 Summary

Observations over the last few years of Run II have shown that the important parameters that can control the impact of beam-beam interactions are: smooth helices (too small or too large beam separations need to be avoided), small beam emittances, low machine chromaticity, proper choice of machine tunes, and low machine coupling.

Transfer efficiencies in the Tevatron at the start of Run II were severely limited by beam-beam effects. The major losses were those of anti-protons during the squeeze. Smaller but significant anti-proton losses also occurred at 150 GeV and during acceleration. Most of these losses were overcome by changing the helices to increase the beam separations, with smaller anti-proton emittances and by operating at lower chromaticities. Large proton losses and large emittance growth of anti-protons at the start of stores have been corrected mainly by adjustments of the tunes. At present beam-beam related losses reduce the integrated luminosity by 16-24%: 2% due to losses at 150 GeV, 6-8% during acceleration and squeeze, and 8-16% due to losses at the start of collisions. There is therefore room for further improvement, especially during the acceleration and during the early part of a store.

Anti-proton intensities are expected to increase about 3-4 fold during the Run II upgrade. Strong-strong effects due to the beam-beam interactions could start to become important. Careful control of beam losses at all stages of the Tevatron operational cycle will continue to be required.

Understanding and mitigating the effects of the beam-beam interactions in the Tevatron has been made possible by the dedicated work of several colleagues including (but not limited to): Y. Alexahin, J. Annala, B. Erdelyi, N. Gelfand, A. Jansson, J. Johnstone, V. Lebedev, P. Lebrun, M. Martens, R. Pasquinelli, R. Moore, V. Shiltsev, D. Still, M. Syphers, C.Y. Tan, A. Valishev, M. Xiao, X.L. Zhang (at Fermilab), and F. Schmidt, F. Zimmermann (at CERN) as well as colleagues at BNL, LBL and SLAC.

References

- [1] V. Shiltsev, Proceedings of EPAC 2004
- [2] T. Sen, B. Erdelyi, M. Xiao, V. Boochoa, *Beam-beam effects at the Fermilab Tevatron: theory*, PRSTAB April 2004
- [3] A. Kabel et al. Proceedings of PAC03, pg 3542
J. Qiang et al., Proceedings of PAC03, pg 3401
- [4] <http://waldo.fnal.gov/~tsen/BBCODE/public/>
- [5] T. Sen, Proceedings of PAC 2003, pg 34
- [6] X.L. Zhang et al., Proceedings of PAC 2003, pg 1757
- [7] <http://beamdocs.fnal.gov>
- [8] Y. Alexahin, FNAL report Beams-doc-802-v1 (2003)
- [9] T. Sen et al., Proceedings of PAC 2003, pg 1754
- [10] R.J. Pasquinelli et al., Proceedings of PAC 2003, pg 3068
A. Jansson et al., Proceedings of EPAC 2004
P. Lebrun, FNAL report Beams-doc-1275-v1 (2004)
- [11] H. Cheung et al, Proceedings of PAC 2003, pg 2488
- [12] T. Sen, FNAL report Beams-doc-689 (2003)
- [13] A. Tollestrup et al., Proceedings of PAC 2003, pg 2497
- [14] J.P. Koutchouk, LHC Project Note 223 (2000)
J.P. Koutchouk, J. Wenninger and F. Zimmermann, Proceedings of EPAC 2004
- [15] B. Erdelyi and T. Sen, FNAL report Fermilab-TM-2268-AD (2004)